Fire-climate interactions through aerosol radiative effect in a global chemistry-climate-vegetation model

Chenguang Tian[1, 2], Xu Yue[1], Jun Zhu[1], Hong Liao[1], Yang Yang[1], Yadong Lei[3], Xinyi Zhou[1], Hao Zhou[2], Yimain Ma[2], Yang Cao[2]

[1] Jiangsu Key Laboratory of Atmospheric Environment Monitoring and Pollution Control, Collaborative Innovation Center of Atmospheric Environment and Equipment Technology, School of Environmental Science and Engineering, Nanjing University of Information Science & Technology (NUIST), Nanjing, 210044, China

[2] Climate Change Research Center, Institute of Atmospheric Physics, Chinese Academy of Sciences, Beijing, 100029, China

[3] State Key Laboratory of Severe Weather & Key Laboratory of Atmospheric Chemistry of CMA, Chinese Academy of Meteorological Sciences, Beijing, 100081, China

Corresponding author: Xu Yue (Email: yuexu@nuist.edu.cn)

Abstract

Fire emissions influence radiation, climate, and ecosystems through aerosol radiative effects. These can drive rapid atmospheric and land surface adjustments which feed back to affect fire emissions. However, the magnitude of such feedback remains unclear on the global scale. Here, we quantify the impacts of fire aerosols on radiative forcing and the fast atmospheric response through direct, indirect, and albedo effects based on the two-way simulations using a well-established chemistry-climate-vegetation model. Globally, fire emissions cause a reduction of 0.565 ± 0.166W m^{-2} in net radiation at the top of the atmosphere with dominant contributions by aerosol indirect effect (AIE). Consequently, terrestrial surface air temperature decreases by 0.061 ± 0.165 °C with coolings of >0.25°C over eastern Amazon, western U.S., and boreal Asia. Both aerosol direct effect (ADE) and AIE contribute to such cooling while the aerosol albedo effect (AAE) exerts an offset warming, especially at high latitudes. Land precipitation decreases by 0.180 ± 0.966 mm $month^{-1}$ (1.78 ± 9.56%) mainly due to the inhibition in central Africa by AIE. Such rainfall deficit further reduces regional leaf area index (LAI) and lightning ignitions, leading to changes in fire emissions. Globally, fire emissions reduce by 2%-3% because of the fire-induced fast responses in humidity, lightning, and LAI. The fire aerosol radiative effects may cause larger perturbations to climate systems with likely more fires under global warming.

Short summary

We quantify the impacts of fire aerosols on climate through direct, indirect, and albedo effects. In atmosphere-only simulations, we find global fire aerosols cause surface cooling and rainfall inhibition over many land regions. These fast atmospheric perturbations further lead to a reduction in regional leaf area index and lightning activities. By considering the feedback of fire aerosols on humidity, lightning, and leaf area index, we predict a slight reduction in fire emissions.

Keywords: Fire emissions; radiative effect; climate feedback; ModelE2-YIBs model

1 Introduction

Fire occurs all year round in both hemispheres, burning about 1% of the Earth's surface and emitting roughly 2–3 Pg (=10^{15} g) carbon into atmosphere every year (van der Werf *et al.*, 2017). Fire activities are strongly influenced by fuel availability, ignition/suppression, and climate conditions (Flannigan *et al.*, 2009). The fuel type, continuity, and amount affect fire occurrence and spread probability (Flannigan *et al.*, 2013). Lightning discharge is the most important natural source of fire ignition (Macias Fauria and Johnson, 2006). Human activities affect fire patterns by adding ignition sources or by suppressing processes (Andela *et al.*, 2017). Compared to the above factors, climate shows a more dominant role in modulating fire activities through the changes of fuel moisture and spread conditions (Flannigan and Harrington, 1988).

Fire exerts prominent impacts on Earth systems and human society through various processes. Biomass burning emits a large amount of trace gases and aerosol particles into the troposphere, affecting air quality at the local and downwind regions (Yue and Unger, 2018). *In situ* observations showed that about one-third of the background particles in the free troposphere of North America were originated from biomass burning (Hudson *et al.*, 2004). Extremely intense fires can even inject aerosols into stratosphere, where the particles were transported globally (Yu *et al.*, 2019). Fire-induced air pollution can reduce global terrestrial productivity of unburned forests (Yue and Unger, 2018), leading to weakened carbon uptake by ecosystems. The global transport of fire air pollution also causes large threats to public health by increasing the risks of diseases and mortality (Liu *et al.*, 2015). It is estimated that fire-induced particulate matter causes more than 33,000 deaths globally each year (Chen *et al.*, 2021).

Aerosols from fires can cause substantial impact on climate via radiative effect owing to their different optical and chemical properties (Xu *et al.*, 2021). Aerosol radiative effect represents the fast atmospheric adjustment or response before changing global mean surface air temperature (TAS). First, aerosols scatter and/or absorb solar radiation through aerosol direct effect (ADE), leading to altered energy budget and climate variables (Carslaw *et al.*, 2010). There is no agreement on the sign of ADE of biomass burning aerosols at the global scale. Some studies (Heald *et al.*, 2014; Veira *et al.*, 2015; Zou *et al.*, 2020) predicted positive forcing while others (Ward *et al.*, 2012; Jiang *et al.*, 2016; Grandey *et al.*, 2016) yielded negative forcing (−0.2 to 0.2 W m^{-2}), mainly because of the large uncertainties in the absorption of fire-emitted black carbon (BC) (Carslaw *et al.*, 2010; IPCC,

2014). Second, aerosols can serve as cloud condensation nuclei (CCN) or ice nuclei to affect the microphysical properties of cloud. Such aerosol indirect effect (AIE) further influences climate system through the changes of cloud albedo and lifetime (Twomey, 1974; Albrecht, 1989). Globally, fire aerosols account for ~30% of the total CCN (Andreae *et al.*, 2004) and the overall negative AIE of fire aerosol is stronger than the ADE in magnitude (Liu *et al.*, 2014; Ward *et al.*, 2012; Jiang *et al.*, 2016). Third, deposition of fire-emitted BC aerosols reduces surface albedo and promotes ice/snow melting, which is called aerosol albedo effect (AAE) (Hansen and Nazarenko, 2004; Warren and Wiscombe, 1980). Compared with other two effects, the AAE shows more regional characteristics (Kang *et al.*, 2020). These fire-induced disturbance in radiative fluxes further alter meteorological and hydrologic variables, which in turn affect fire activities through the changes in fuel moisture and weather conditions.

The impacts of fire-induced rapid adjustments on fire activity at the global scale have not been fully assessed. While observations revealed fire-induced perturbations to regional climate (Bali *et al.*, 2017; Zhuravleva *et al.*, 2017), its feedback to fire activities are difficult to be isolated from the influences of background climate. Models provide unique tools to explore fire-climate interactions resulting from aerosol radiative effect especially at the regional to global scales. However, they are not routinely included in most of Earth system models. The IPCC sixth assessment report (AR6) did not provide a quantitative assessment of such feedback as well (IPCC, 2021). In this study, we explore the impacts of fire aerosol radiative effect on climate and the consequent feedbacks to fire emissions by using a well-established fire parameterization coupled to a chemistry-climate-vegetation model ModelE2-YIBs (Yue and Unger, 2015). The main objectives are (1) to isolate the radiative effects of fire aerosols through ADE, AIE, and AAE processes and (2) to quantify the feedback of fire-induced rapid adjustments to fire emissions.

2 Data and methods

2.1 Data

We use the emissions from Global Fire Emission Database version 4.1s (GFED4.1s) to validate the simulated fire emissions. The GFED4.1s provides monthly fire emission fluxes of various air pollutants based on satellite retrieval of area burned from the Moderate Resolution Imaging Spectroradiometer (MODIS) (van der Werf *et al.*, 2017). Area burned in GFED4.1s is mainly

derived from the MODIS burned area product (Giglio *et al.*, 2013), taking into account "small" fires outside the burned area maps based on active fire detections (Randerson *et al.*, 2012). The gridded fire emission dataset has a spatial resolution of 0.25°×0.25° and is available for every month from July 1997. To compute anthropogenic ignition and suppression effects (see section 2.3), we use a downscaled population density dataset from Gao (2017, 2020). Monthly sea surface temperature (SST) and sea ice concentration (SIC) obtained from Hadley Centre Sea Ice and Sea Surface Temperature (HadISST) dataset (Rayner *et al.*, 2003) are used as the boundary conditions for the climate model.

2.2 ModelE2-YIBs model

The chemistry-climate-vegetation model ModelE2-YIBs is used to simulate the two-way coupling between fire aerosols and climate systems. The ModelE2-YIBs is composed of the NASA Goddard Institute for Space Studies (GISS) ModelE2 model (Schmidt *et al.*, 2014) and the Yale Interactive terrestrial Biosphere Model (YIBs) (Yue and Unger, 2015). The GISS ModelE2 is a global climate-chemistry model with a horizontal resolution of 2° × 2.5° latitude by longitude and 40 vertical layers extending to the stratosphere (0.1hPa). The dynamics and physics codes are executed every 30 minutes and the radiation code is calculated every 2.5 hours.

The gas-phase chemistry scheme considers 156 chemical reactions among 51 species, including NO_x−HO_x−O_x−CO−CH_4 chemistry and different species of volatile organic compounds. Aerosol species in ModelE2 include sulfate, nitrate, ammonium, sea salt, dust, BC, and organic carbon (OC), which are interactively calculated and tracked for both mass and number concentrations. Heterogeneous chemistry on dust surfaces and NO_x-dependent secondary organic aerosol production from isoprene and terpenes is included in the model (Bauer *et al.*, 2007b; Tsigaridis and Kanakidou, 2007). The thermodynamic gas-aerosol equilibrium module is used to calculate the phase partitioning of the H_2SO_4/HSO_4^-/SO_4^{-2}−HNO_3/NO_3^-−NH_3/NH_4^+−HCL/CL^-−Na^+−Ca^{2+}−Mg^{2+}−K^+−H_2O system (Metzger *et al.*, 2006; Bauer *et al.*, 2007a). The aerosol microphysical scheme is based on the quadrature method of moments, which incorporates nucleation, gas-particle mass transfer, new particle formation, particle emissions, aerosol phase chemistry, condensational growth, and coagulation (Bauer *et al.*, 2008). The residence time of aerosol species varies greatly in space and time due to different removal rates. Turbulent dry

deposition is determined by resistance-in-series scheme, which is closely coupled to the boundary layer scheme and implemented between the surface layer (10 m) and the ground (Koch *et al.*, 2006). The wet deposition consists of several processes including scavenging within and below cloud, evaporation of falling rainout, transportation along convective plumes, and detrainment and evaporation from convective plumes (Koch *et al.*, 2006; Shindell *et al.*, 2006).

In ModelE2, gases can be converted to aerosols through chemical reactions, while aerosols affect photolysis and provide reaction surface for gases. For example, the formation of sulfate aerosols is driven by modeled oxidants (Bell *et al.*, 2005), and the chemical production of nitrate aerosols is dependent on nitric acid and gaseous ammonia (Bauer *et al.*, 2007b). Moreover, the disturbances of aerosols on climate systems via direct, indirect, and albedo effects are considered in ModelE2. Aerosol optical parameters are calculated by the Mie scattering theory using complex refractive index depending on chemical speciation and particle size. The first AIE is estimated by the prognostic treatment of cloud droplet number concentration, which is a function of species-dependent contact nucleation, auto-conversion, and immersion freezing (Menon *et al.*, 2008; Menon *et al.*, 2010). The AAE of BC is considered by estimating the decline of surface albedo as a function of aerosol concentrations at the top layer of snow or ice (Koch and Hansen, 2005). We note that average BC deposition to snow estimated by measurement-based average scavenging ratios is used as a climatological proxy to the physical process of BC deposition (Hansen and Nazarenko, 2004). The latter involves size resolved and meteorologically dependent BC deposition fluxes, as would be found in a chemical transport model, but is not used here due to computational constraints. More detailed descriptions of ModelE2 can be found in Schmidt *et al.* (2014). It has been extensively evaluated for meteorological and chemical variables against observations, reanalysis products and other models, and widely used for studies of climate systems, atmospheric components, and their interactions (Schmidt *et al.*, 2014).

YIBs is a process-based vegetation model that dynamically simulates tree growth and terrestrial carbon fluxes with prescribed fractions of nine plant functional types (PFTs), including deciduous broadleaf forest, evergreen needleleaf forest, evergreen broadleaf forest, tundra, shrubland, C_3/C_4 grassland, and C_3/C_4 cropland. Essential biological processes such as photosynthesis, phenology, autotrophic and heterotrophic respiration are considered and parameterized using the state-of-the-art schemes (Yue and Unger, 2015). Dynamic daily leaf area

index (LAI) is estimated based on carbon allocation which is updated every 10 days and prognostic phenology which is dependent instantaneously on temperature and drought conditions. Simulated tree height, phenology, gross primary productivity and LAI agree well with site-level observations and/or satellite retrievals (Yue and Unger, 2015). The YIBs model joined the dynamic global vegetation model inter-comparison project TRENDY and showed reasonable performance of carbon fluxes against available observations (Friedlingstein *et al.*, 2020). In the coupled model, ModelE2 provides meteorological drivers to YIBs, which feeds back to alter land surface water and energy fluxes through changes in stomatal conductance, surface albedo, and LAI. By incorporating YIBs into ModelE2, the new coupled model ModelE2-YIBs can simulate interactions between terrestrial ecosystems and climate systems through the exchange of water and energy fluxes, and chemical components (Yue and Unger, 2015; Yue *et al.*, 2017).

2.3 Fire parameterization

We implemented the active global fire parameterization from Pechony and Shindell (2009) into ModelE2-YIBs model. The parameterization considers key fire-related processes including fuel flammability, lightning and human ignitions, and human suppressions. Flammability is a unitless metric indicating conditions favorable for fire occurrence, and is calculated using vapor pressure deficit (VPD, hPa), precipitation (R, mm day^{-1}), and LAI (m^2 m^{-2}) as follows:

$$\mathrm{Flam} = \mathrm{VPD} \times \mathrm{LAI} \times \mathrm{e}^{-\mathrm{c_R} \times \mathrm{R}} \quad (1)$$

Here, LAI represents vegetation density and is dynamically calculated by YIBs model. $\mathrm{c_R}$ is a constant set to 2. VPD is a vital indicator of flammability conditions:

$$\mathrm{VPD} = \mathrm{e_s} \times \left(1 - \frac{\mathrm{RH}}{100}\right) \quad (2)$$

where $\mathrm{e_s}$ is the saturation vapor pressure and RH is surface relative humidity. $\mathrm{e_s}$ can be calculated by Goff-Gratch equation:

$$\mathrm{e_s} = \mathrm{e_{st}} \times 10^{\mathrm{Z}} \quad (3)$$

where $\mathrm{e_{st}}$ is 1013.246 hPa and

$$\mathrm{Z} = \mathrm{a} \times \left(\frac{\mathrm{T_s}}{\mathrm{T}} - 1\right) + \mathrm{b} \times \log\frac{\mathrm{T_s}}{\mathrm{T}} + \mathrm{c} \times \left(10^{\mathrm{d}\left(1-\frac{\mathrm{T_s}}{\mathrm{T}}\right)} - 1\right) + \mathrm{f} \times \left(10^{\mathrm{h}\left(\frac{\mathrm{T_s}}{\mathrm{T}}-1\right)} - 1\right) \quad (4)$$

Here, a, b, c, d, f and h are constants set to -7.90298, 5.02808, -1.3816×10^{-7}, 11.344, 8.1328×10^{-3} and -3.49149, respectively. $\mathrm{T_s}$ is boiling point of water and equal to 373.16 K. VPD and LAI in Eq.

(1) are calculated in half-hourly and daily time step, respectively, while 30-day running average precipitation is employed to avoid unrealistically huge flammability fluctuations. It should be noted that the response of flammability to abovementioned factors may not be instantaneous, but may occur over time. For example, a reduction in precipitation in one season at a given location may reduce foliage growth and hence reduce the fuel available for combustion in another season.

Natural and anthropogenic ignition rate determines whether the fire can actually occur. If the ignition rate is zero, the resulting fire emissions will be zero, regardless of flammability. The natural ignition rate I_N depends on cloud-to-ground lightning (CoGL) rate, which is simulated by ModelE2 following the parameterization of Price and Rind (1994):

$$I_N = \mathrm{CoGL} = \begin{cases} 3.44 \times 10^{-5} \times H^{4.9} & \text{over land} \\ 6.4 \times 10^{-4} \times H^{1.73} & \text{over ocean} \end{cases} \quad (5)$$

where H is the cloud depth (unit: km).

Humans influence fire activity by adding ignition sources and suppressing fire events, the rates of which increase with population and to some extent counteract each other. The anthropogenic ignition rate I_A (number km^{-2} month^{-1}) is calculated as follows (Venevsky *et al.*, 2002):

$$I_A = k(PD) \times PD \times \alpha \quad (6)$$

where PD is population density (number km^{-2}). $k(PD) = 6.8 \times PD^{-0.6}$ stands for ignition potentials of human activity, assuming that people in scarcely populated areas interact more with the natural ecosystems and therefore produce more ignition potential. α is the number of potential ignitions per person per month and set to 0.03.

In principle, the successful suppression of fires is dependent on early detection. It is reasonably assumed that fires are detected earlier and suppressed more effectively in highly populated areas. Therefore, the fraction of non-suppressed fires F_{NS} can be expressed as:

$$F_{NS} = c_1 + c_2 \times \exp(-\omega \times PD) \quad (7)$$

where c_1, c_2 and ω are constants and set to 0.05, 0.95 and 0.05, respectively. The selection of constant values in Eq. (7) is done in a heuristic way, due to lack of quantified data globally. It assumes that up to 95% of fires is suppressed in the densely populated regions but only 5% in unpopulated areas.

With the calculation of flammability (Flam), ignition (I_N and I_A), and non-suppression (F_{NS}), the fire count density N_{fire} (unit: number km^{-2}) at a specific time step can be derived as:

$$N_{fire} = Flam \times (I_N + I_A) \times F_{NS} \quad (8)$$

Finally, fire emissions of trace gases and particulate matters (FireEmis) are calculated as:

$$FireEmis = N_{fire} \times EF \quad (9)$$

Here, EF is the PFT-specific emission factor of an air pollutant such as BC, OC, NO_x, NH_3, SO_2, CO, Alkenes and Paraffin. For each species, simulated gridded emissions are grouped by dominant PFT and compared to annual total emissions from GFED4.1s over the same grids. The EF is then calibrated to minimize the root-mean-square error between the simulated and GFED data for all land grids. Such calibration adjusts only the global total amount of fire emissions without changing the spatiotemporal pattern predicted by the parameterization. The EF is the intrinsic attribution of wildfire emissions that should not vary greatly with climatic conditions. The fire-emitted minerals or dust-like materials are not implemented in the current model, given that these species is not included in the current GFED4.1s.

Compared to fire indexes, such as Canadian Fire Weather Index system (Wagner, 1987), this fire parameterization shows advantages in integrating the effects of meteorology, vegetation, natural ignition, and human activities (both ignition and suppression) on fires. Furthermore, it is physically straightforward and has been validated based on global observations (Pechony and Shindell, 2009; Hantson *et al.*, 2020). In ModelE2-YIBs, fire emissions are affected by environmental factors following above parameterizations. In turn, the radiative effects of fire-emitted aerosols feed back to affect those climatic and ecological factors. Note that the changes in the environmental factors may result in changes to fire emissions later. We consider only the fire emissions at surface due to the large uncertainties in depicting fire plume height (Sofiev *et al.*, 2012; Ke *et al.*, 2021). The fire emissions include both primary aerosols and trace gases, the latter of which react with other species to form the secondary aerosols. These particles could be transported across the globe by the three-dimensional atmospheric circulation and eventually removed through either dry or wet deposition.

2.4 Simulations

We perform four groups of sensitivity experiments (Table 1) with the ModelE2-YIBs model to quantify the fire-climate interactions through different radiative processes. The first group with suffix ‘AD’ considers only the ADE. The second (third) group with suffix ‘AD_AI’ (‘AD_AA’)

considers both ADE and AIE (ADE and AAE). The fourth group with suffix 'AD_AI_AA' includes all three aerosol radiative effects (ADE, AIE, and AAE). Within each group, two runs are performed with (YF) or without (NF) fire emissions. For YF simulations, fire-induced aerosols including primarily emitted and secondarily formed are dynamically calculated based on fire parameterization (see section 2.3) and atmospheric transport. These fire emissions cause radiative perturbations and the consequent fast atmospheric adjustments, which feed back to influence fire emissions. For NF simulations, fire emissions are calculated offline at each step without perturbing the climate system, which can be considered that there is no fire emission. By comparing the climatic variables from the YF and NF runs in the first group, we isolate the impacts of fire aerosols on climate through ADE. By comparing the climatic effects from the first and second (third) groups, we isolate the AIE (AAE) of fire aerosols. By comparing the climatic variables from YF and NF runs in the fourth group, the overall effect (ADE+AIE+AAE) is obtained. Besides, the differences of fire emissions between simulations of "YF_AD_AI_AA" and "NF_AD_AI_AA" represent the feedback of fire aerosol-induced environmental perturbations. Note that fire-emitted gas-phase species also perturb radiation via atmospheric absorption and/or feedback from rapid adjustment; these perturbations are far less than aerosol forcing and could be ignored.

For each simulation, climatological mean CO_2 concentrations, SST/SIC, and population density during 1995-2005 are used as boundary conditions to drive the model. Such configuration ignores the year-to-year variability in climate systems, which may cause significant changes in annual fire emissions (Burton *et al.*, 2020). Each simulation is integrated for 25 years with the first 5 years spinning up and the last 20 years averaged. A two-tailed Student t-test is performed to assess 90% confidence levels of the predicted radiative and climatic responses ($p < 0.1$). The global mean or sum value is depicted in the form of mean value $\pm$ standard deviation. In this study, downward (upward) radiative/heat fluxes are defined as positive (negative). Given that the model is driven by prescribed SST and SIC, only the rapid adjustments of atmospheric variables are taken into account and we mainly focus on climate changes over land grid. The radiative effect simulated with such model configuration is termed the effective radiative forcing (IPCC, 2014).

3 Results

3.1 Model evaluation

Simulated fire emissions of BC and OC show hotspots in the tropics, such as Amazon, Sahel, central Africa, and Southeast Asia (Fig. S1). The large tropical fire emissions are related to abundant vegetation and/or distinct dry seasons. Compared to GFED4.1s data, ModelE2-YIBs slightly underestimates boreal fire emissions especially over northern Asia and North America. On the global scale, fire releases 1.85 ± 0.01 Tg (1 Tg = 10^{12} g) C $year^{-1}$ of BC and 16.8 ± 0.92 Tg C $year^{-1}$ of OC in ModelE2-YIBs, close to the 1.86 Tg C $year^{-1}$ of BC and 16.4 Tg C $year^{-1}$ of OC estimated by GFED4.1s. In general, ModelE2-YIBs reasonably captures the spatial distribution of fire emissions, with high spatial correlations of 0.67 ($p < 0.01$) for BC and 0.58 ($p < 0.01$) for OC, and low normalized mean biases of 0.6% for BC and 2.4% for OC against satellite-based observations.

3.2 Fire-induced radiative perturbations

Fig. S2 shows the fire-induced changes in Aerosol Optical Depth (AOD) at 550nm. Fire emissions largely enhance surface aerosols especially over tropical regions. Hotspots are located in southern Africa and South America with regional enhancement larger than 0.05. In addition, large enhancement is also found at boreal high latitudes (> 0.01). At the global scale, fires enhance AOD by 0.006 ± 0.001 with 0.010 ± 0.001 over land.

Fire aerosols cause large perturbations in net radiation at top of atmosphere (TOA). Globally, the net radiation at TOA decreases 0.565 ± 0.166 W m^{-2} by fire aerosols (Fig. 1a). Regionally, negative changes are predicted over central Africa, western South America, western North America and the boreal high latitudes. Diagnosis shows that fire-induced AIE dominates the reduction of TOA flux with a global value of -0.440 ± 0.264 W m^{-2} (Fig. 1c), accounting for 78% of the total TOA radiative effect by fire aerosols. The spatial correlation coefficient is 0.62 over land grids between the perturbations by all aerosol effects and that by AIE alone. Compared to AIE, the changes in TOA radiative fluxes are much smaller for fire ADE (-0.058 ± 0.213W m^{-2}, Fig. 1b) and AAE (-0.016 ± 0.283 W m^{-2}, Fig. 1d) with limited perturbations on land.

Fire aerosols decrease net shortwave radiation reaching the surface up to 9 W m^{-2} in central Africa and 7 W m^{-2} in Amazon (Fig. 2a), where biomass burning emissions are most intense (Fig. S1). Such pattern is in general consistent with the changes of TOA fluxes (Fig. 1a), leading to an average reduction of -1.227 ± 0.216 W m^{-2} in the shortwave radiation over global land. The fire-induced ADE alone reduces land surface shortwave radiation by 0.654 ± 0.353 W m^{-2} with the

maximum center in Amazon (Fig. S3a). As a comparison, the fire-induced AIE causes a smaller reduction of -0.553 ± 0.518 W m^{-2} with the hotspot in central Africa (Fig. S3c). The net effect of AAE (0.263 ± 0.551 W m^{-2}) by fire aerosols is positive mainly because fire AAE reduces surface albedo and increase shortwave radiation over Tibetan Plateau and boreal high latitudes (Fig. S3e). However, the magnitude of AAE is much smaller compared to that of ADE and AIE.

Changes in surface longwave radiation (Fig. 2b) are much smaller than those in shortwave radiation (Fig. 2a). Regionally, positive changes are predicted in the western U.S., eastern Amazon, and South Africa, where fire-induced surface cooling (Fig. 3a) decreases the upward longwave radiation. On the global scale, fire aerosols cause a decrease of 0.281 ± 0.371 W m^{-2} in surface upward longwave radiation. As a result, fire aerosols induce a net atmospheric absorption of 0.191 ± 0.227 W m^{-2} over land grids (Fig. 2c). The reductions in surface shortwave radiation are largely balanced by changes in heat fluxes at the surface, which shows an average decrease of 0.826 ± 0.311 W m^{-2} in the upward fluxes over land grids (Fig. 2d). Fire ADE and AIE lead to reductions of 0.503 ± 0.289 W m^{-2} and 0.432 ± 0.411W m^{-2} in surface upward heat fluxes, respectively (Fig. S3b and S3d). Changes in sensible heat account for 82.2 % of the changes in total heat reduction, much higher than the contributions of 17.8% by latent heat fluxes (Fig. S4). Regionally, the upward sensible heat decreases in the western U.S. and Amazon mainly due to fire ADE, while the upward latent heat decreases in central Africa mainly by fire AIE (Fig. S5).

3.3 Fire-induced fast climatic responses

In response to the perturbations in radiative fluxes, land TAS decreases 0.061 ± 0.165 °C globally by fire aerosols (Fig. 3a). Such cooling is mainly located in western U.S., Amazon, and boreal Asia, following the large reductions in shortwave radiation (Fig. 2a). Meanwhile, moderate warming is predicted at the high latitudes of both hemispheres especially over the areas covered with land ice such as Greenland and Antarctica. Sensitivity experiments show that both ADE (Fig. 4a) and AIE (Fig. 4c) of fire aerosols result in net cooling globally, with regional reductions of TAS over boreal Asia and North America. In contrast, the fire AAE causes increases of TAS over boreal Asia and North America (Fig. 4e), where the deposition of BC aerosols reduces surface albedo. Consequently, the fire AAE results in a global warming of 0.054 ± 0.163°C, which in part offsets the cooling effects by the ADE and AIE of fire aerosols.

Meanwhile, global land precipitation decreases by 0.180 ± 0.966 mm/month (1.78 ± 9.56%) with great spatial heterogeneity (Fig. 3b). Decreased precipitation is predicted over central Africa, boreal North America, and eastern Siberia. In contrast, increased rainfall is predicted in western U.S., eastern Amazon, and northern Asia. The reduction of precipitation is mainly contributed by fire AIE, which reduces cloud droplet size and inhibits local rainfall in central Africa (Fig. 4d). Consequently, latent heat fluxes are reduced to compensate the rainfall deficit in central Africa (Fig. S4b).

3.4 Fast response feedback on fire emissions

The fire-aerosol-induced fast response in precipitation, VPD, lightning, and LAI can feed back to affect fire emissions. However, these changes may have contrasting impacts on fire activities. For example, the aerosol-induced reduction of precipitation in central Africa (Fig. 3b) increases local VPD (Fig. 5a) and consequently causes more fire emissions. Meanwhile, such enhanced drought condition inhibits plant growth and decreases local LAI (Fig. 5c), which has negative impacts on fire emissions by reducing fuel density. Furthermore, the fire AIE inhibits the development of convective cloud, which limits cloud height and the number of cloud-to-ground lightning in central Africa (Fig. 5b), leading to reduced ignition sources and fire emissions.

To illustrate the joint the impacts of fire-aerosol-induced fast climate responses, we count the number out of the four factors contributing positive effects to fire emissions over land grids (Fig. 5d). The larger (smaller) number indicates higher possibility of increasing (decreasing) fire emissions. Most of areas show neutral number of 2, indicating offsetting effects of the changes in fire-prone factors. Only 13.5 % of land grids show numbers higher than 2 with sparse distribution. In contrast, 32.1 % of land grids show numbers smaller than 2, especially for the grids over Siberia and western U.S. where the increased rainfall (Fig. 3b) and decreased VPD (Fig. 5a) inhibit fire emissions. Furthermore, the regional reductions in lightning ignition or LAI promote the inhibition effects. As a result, fire emissions in YF_AD_AI_AA slightly decrease by 31.0 ± 35.9 Gg $year^{-1}$ (1.7%) for BC and 493.6 ± 566.8 Gg $year^{-1}$ (2.9%) for OC compared to NF_AD_AI_AA in which fire emissions do not perturb climate (Fig. 6).

4 Conclusions and discussion

We used the chemistry-climate-vegetation coupled model ModelE2-YIBs to quantify fire-climate interactions through ADE, AIE, and AAE. Globally, fire aerosols decrease TOA net radiation by 0.565 ± 0.166 W m^{-2}, dominated by the AIE over central Africa. Surface net solar radiation also exhibits widespread reductions especially over fire-prone areas with compensations from the decreased sensible and latent heat fluxes. Following the changes in radiation, land TAS decreases by 0.061 ± 0.165 °C and precipitation decreases by 0.180 ± 0.966 mm/month, albeit with regional inconsistencies. The surface cooling is dominated by fire ADE and AIE, while the drought tendency is mainly contributed by fire AIE with hotspots in central Africa. AAE also plays an important role by introducing warming tendency at the mid-to-high latitudes. These fire-induced fast climatic responses further affect VPD, LAI, and lightning ignitions, leading to reductions in global fire emissions of BC by 2% and OC by 3%. It may seem counter-intuitive that reduced precipitation would decrease wildfire emissions, while the observation-based data show that the fire-precipitation correlations are not negative in all regions (Fig. S6). In this study, the inhibition of precipitation in central Africa (Fig. 3b) reduces regional LAI (Fig. 5c) and decreases fuel availability for fire occurrence, resulting in a positive correlation between fire and precipitation that matches the observed relationship in Africa (Fig. S6). However, in North America, Eurasia, and the Amazon Basin, precipitation is anti-correlated with fire emissions. These differences may reflect the seasonal variation of rainfall in the different regions.

Our predicted reduction of 0.565 ± 0.166 W m^{-2} in TOA radiation by fire aerosols is close to the estimate of -0.51 W m^{-2} reported by Jiang *et al.* (2016) and -0.59 W m^{-2} of Zou *et al.* (2020) using different models with prescribed SST/SIC and fire-induced ADE, AIE and AAE (Table 2). Within such change, fire ADE alone makes a moderate contribution of -0.016 ± 0.283 W m^{-2}, falling within the range of -0.2 to 0.2 W m^{-2} from other studies. The large uncertainty of fire ADE is likely related to the discrepancies in the BC absorption among climate models, which cause varied net effects when offsetting the radiative perturbations of scattering aerosols. As a comparison, fire AIE in our model induces a significant radiative effect of -0.440 ± 0.264 W m^{-2}. However, such magnitude is much smaller than previous estimates of -0.7 to -1.1 W m^{-2} using different models (Table 2). We further estimated a limited fire AAE of -0.016 ± 0.283 W m^{-2}, consistent with previous findings showing insignificant role of AAE by fire aerosols (Ward *et al.*, 2012; Jiang *et al.*, 2016). Our estimates of reductions in TAS and precipitation also fall within the range of previous studies

(Table 2).

Our estimates are subject to some limitations and uncertainties. First, we considered only the fast climatic responses of land surface with prescribed SST and SIC in the simulations. Although most of fire-induced AOD changes are located on land (Fig. S2), the air-sea interaction may cause complex climatic responses to aerosol radiative effects. In a recent study, Jiang *et al.* (2020) emphasized the role of slow feedback contributed by fire aerosols on global precipitation reduction by using a coupled model. Such air-sea interaction will modify the magnitude and/or spatial pattern of fast climatic responses revealed in this study, and should be explored in the future studies with coupled ocean models. Second, the nonlinear effects of different radiative processes may influence the attribution results. In this study, we isolate the effects of AIE and AAE by subtracting variables between different groups following the approaches by Bauer and Menon (2012). However, the additive perturbations from individual processes are not equal to the total perturbations with all processes in one simulation. For example, the sum of three processes causes changes of TOA radiation by -0.513 ± 0.324 W m^{-2} (Figs 1b-1d), surface temperature by -0.037 ± 0.160 °C (Figs 4a, 4c, 4e), and precipitation by -1.090 ± 1.122 mm $month^{-1}$ (Figs 4b, 4d, 4f). These perturbations are weaker than the net effects of 0.565 ± 0.166 W m^{-2} (Fig. 1a) in radiation and -0.061 ± 0.165 °C in temperature (Fig. 3a), but much stronger than that of -0.18 ± 0.96 mm $month^{-1}$ in precipitation (Fig. 3b) predicted by the simulation with all three processes. As a result, the nonlinear feedbacks among different radiative processes may magnify or offset the final climatic responses to fire aerosols. Third, considering the complex nature of fire activities, the fire parameterization in this study does not incorporate all fire-related processes (e.g., the influence of wind). In addition, the simulations omit several factors influencing fire emissions (e.g., moist content of fuels) and aerosol radiative effects (e.g. fire plume height). For example, studies show significant impacts of plume rise on the vertical distribution of fire aerosols and the consequent radiative effects (Walter *et al.*, 2016). The impacts of human activity on fire emissions are calculated as a function of population density without considerations of differences in economy, education, and policies. These auxiliary factors may increase the spatial heterogeneity of fire aerosol radiative effects and deserve further explorations in the future studies.

Despite these limitations, we made the first attempt to assess the two-way interaction between fire emissions and climate via aerosol radiative effects. Our results show that fire-emitted aerosols

cause negative ERF of 0.565 ± 0.166 W m^{-2}, which is about 20% of the anthropogenic ERF due to the increased greenhouse gases and aerosols from 1950 to 2019 (IPCC, 2021). Such fire ERF largely reduces regional TAS and precipitation, leading to further changes in fire emissions. Although the reduction of 2% to 3% in fire emissions by the fire-climate interaction through aerosol radiative effect seems limited, such change is a result of several complex feedbacks that may exert offsetting effects, and the relative magnitude of individual factors may vary spatially. Both the number of factors and the magnitude of their effects will determine the overall response. Furthermore, our simulations reveal a strong inhibition effect of fire aerosols on LAI in central Africa due to the aerosol-induced drought intensification. Such negative effects on ecosystems are inconsistent with previous estimates that showed certain fertilization effects by fire aerosols (Yue and Unger, 2018), mainly because the rainfall deficit overweighs the diffuse fertilization effects of aerosols. With likely more fires under global warming (Abatzoglou *et al.*, 2019), our results suggested complex and uncertain perturbations by fire emissions to climate and ecosystem through fire-climate interactions.

Acknowledgements

The authors are grateful to Dr. Matthew Kasoar and another anonymous reviewer for their constructive comments that have improved this study.

Financial support

This research was supported by the National Key Research and Development Program of China (grant no. 2019YFA0606802).

Competing Interests

The authors declare that they have no conflict of interest.

Data availability

Hadley Centre Sea Ice and Sea Surface Temperature dataset were obtain from https://www.metoffice.gov.uk/hadobs/hadisst/. Population data could be downloaded form https://cmr.earthdata.nasa.gov/search/concepts/C1739468823-SEDAC.html. GFED data were obtained from https://daac.ornl.gov/VEGETATION/guides/fire_emissions_v4_R1.html. Model

data from this study are available from the corresponding author upon request.

Reference:

Abatzoglou J T, Williams A P and Barbero R 2019 Global Emergence of Anthropogenic Climate Change in Fire Weather Indices *Geophysical Research Letters* **46** 326-36

Albrecht B A 1989 Aerosols, Cloud Microphysics, and Fractional Cloudiness **245** 1227-30

Andela N, Morton D C, Giglio L, Chen Y, van der Werf G R, Kasibhatla P S, DeFries R S, Collatz G J, Hantson S, Kloster S, Bachelet D, Forrest M, Lasslop G, Li F, Mangeon S, Melton J R, Yue C and Randerson J T 2017 A human-driven decline in global burned area *Science* **356** 1356

Andreae M O, Rosenfeld D, Artaxo P, Costa A A, Frank G P, Longo K M and Silva-Dias M A F 2004 Smoking Rain Clouds over the Amazon **303** 1337-42

Bali K, Mishra A K and Singh S 2017 Impact of anomalous forest fire on aerosol radiative forcing and snow cover over Himalayan region *Atmospheric Environment* **150** 264-75

Bauer S E, Koch D, Unger N, Metzger S M, Shindell D T and Streets D G 2007a Nitrate aerosols today and in 2030: a global simulation including aerosols and tropospheric ozone *Atmos. Chem. Phys.* **7** 5043-59

Bauer S E and Menon S 2012 Aerosol direct, indirect, semidirect, and surface albedo effects from sector contributions based on the IPCC AR5 emissions for preindustrial and present-day conditions **117**

Bauer S E, Mishchenko M I, Lacis A A, Zhang S, Perlwitz J and Metzger S M 2007b Do sulfate and nitrate coatings on mineral dust have important effects on radiative properties and climate modeling? **112**

Bauer S E, Wright D L, Koch D, Lewis E R, McGraw R, Chang L S, Schwartz S E and Ruedy R 2008 MATRIX (Multiconfiguration Aerosol TRacker of mIXing state): an aerosol microphysical module for global atmospheric models *Atmos. Chem. Phys.* **8** 6003-35

Bell N, Koch D and Shindell D T 2005 Impacts of chemistry-aerosol coupling on tropospheric ozone and sulfate simulations in a general circulation model **110**

Burton C, Betts R A, Jones C D, Feldpausch T R, Cardoso M and Anderson L O 2020 El Niño Driven Changes in Global Fire 2015/16 **8**

Carslaw K S, Boucher O, Spracklen D V, Mann G W, Rae J G L, Woodward S and Kulmala M 2010 A review of natural aerosol interactions and feedbacks within the Earth system *Atmos. Chem. Phys.* **10** 1701-37

Chen G, Guo Y, Yue X, Tong S, Gasparrini A, Bell M L, Armstrong B, Schwartz J, Jaakkola J J K, Zanobetti A, Lavigne E, Nascimento Saldiva P H, Kan H, Royé D, Milojevic A, Overcenco A, Urban A, Schneider A, Entezari A, Vicedo-Cabrera A M, Zeka A, Tobias A, Nunes B, Alahmad B, Forsberg B, Pan S-C, Íñiguez C, Ameling C, De la Cruz Valencia C, Åström C, Houthuijs D, Van Dung D, Samoli E, Mayvaneh F, Sera F, Carrasco-Escobar G, Lei Y, Orru H, Kim H, Holobaca I-H, Kyselý J, Teixeira J P, Madureira J, Katsouyanni K, Hurtado-Díaz M, Maasikmets M, Ragettli M S, Hashizume M, Stafoggia M, Pascal M, Scortichini M, de Sousa Zanotti Stagliorio Coêlho M, Valdés Ortega N, Ryti N R I, Scovronick N, Matus P, Goodman P, Garland R M, Abrutzky R, Garcia S O, Rao S, Fratianni S, Dang T N, Colistro V, Huber V, Lee W, Seposo X, Honda Y, Guo Y L, Ye T, Yu W, Abramson M J, Samet J M and Li S 2021 Mortality risk attributable to wildfire-related PM_{2·5} pollution: a global time series study in 749 locations *The Lancet Planetary Health* **5** e579-e87

Flannigan M, Cantin A S, de Groot W J, Wotton M, Newbery A and Gowman L M 2013 Global wildland fire season severity in the 21st century *Forest Ecology and Management* **294** 54-61

Flannigan M and Harrington J B 1988 A Study of the Relation of Meteorological Variables to Monthly Provincial Area Burned by Wildfire in Canada (1953–80) *Journal of Applied Meteorology and Climatology* **27** 441-52

Flannigan M, Krawchuk M A, de Groot W J, Wotton B M and Gowman L M 2009 Implications of changing climate for global wildland fire %J International Journal of Wildland Fire **18** 483-507

Friedlingstein P, O'Sullivan M, Jones M W, Andrew R M, Hauck J, Olsen A, Peters G P, Peters W, Pongratz J, Sitch S, Le Quéré C, Canadell J G, Ciais P, Jackson R B, Alin S, Aragão L E O C, Arneth A, Arora V, Bates N R, Becker M, Benoit-Cattin A, Bittig H C, Bopp L, Bultan S, Chandra N, Chevallier F, Chini L P, Evans W, Florentie L, Forster P M, Gasser T, Gehlen M, Gilfillan D, Gkritzalis T, Gregor L, Gruber N, Harris I, Hartung K, Haverd V, Houghton R A, Ilyina T, Jain A K, Joetzjer E, Kadono K, Kato E, Kitidis V, Korsbakken J I, Landschützer P, Lefèvre N, Lenton A, Lienert S, Liu Z, Lombardozzi D, Marland G, Metzl N, Munro D R, Nabel J E M S, Nakaoka S I, Niwa Y, O'Brien K, Ono T, Palmer P I, Pierrot D, Poulter B, Resplandy L, Robertson E, Rödenbeck C, Schwinger J, Séférian R, Skjelvan I, Smith A J P, Sutton A J, Tanhua T, Tans P P, Tian H, Tilbrook B, van der Werf G, Vuichard N, Walker A P, Wanninkhof R, Watson A J, Willis D, Wiltshire A J, Yuan W, Yue X and Zaehle S 2020 Global Carbon Budget 2020 *Earth Syst. Sci. Data* **12** 3269-340

Gao J 2017 Downscaling Global Spatial Population Projections from 1/8-degree to 1-km Grid Cells.

Gao J 2020 Global 1-km Downscaled Population Base Year and Projection Grids Based on the Shared Socioeconomic Pathways, Revision 01. (Palisades, NY: NASA Socioeconomic Data and Applications Center (SEDAC))

Giglio L, Randerson J T and van der Werf G R 2013 Analysis of daily, monthly, and annual burned area using the fourth-generation global fire emissions database (GFED4) *Journal of Geophysical Research: Biogeosciences* **118** 317-28

Grandey B S, Lee H H and Wang C 2016 Radiative effects of interannually varying vs. interannually invariant aerosol emissions from fires *Atmos. Chem. Phys.* **16** 14495-513

Hansen J and Nazarenko L 2004 Soot climate forcing via snow and ice albedos **101** 423-8

Hantson S, Kelley D I, Arneth A, Harrison S P, Archibald S, Bachelet D, Forrest M, Hickler T, Lasslop G, Li F, Mangeon S, Melton J R, Nieradzik L, Rabin S S, Prentice I C, Sheehan T, Sitch S, Teckentrup L, Voulgarakis A and Yue C 2020 Quantitative assessment of fire and vegetation properties in simulations with fire-enabled vegetation models from the Fire Model Intercomparison Project *Geosci. Model Dev.* **13** 3299-318

Heald C L, Ridley D A, Kroll J H, Barrett S R H, Cady-Pereira K E, Alvarado M J and Holmes C D 2014 Contrasting the direct radiative effect and direct radiative forcing of aerosols *Atmos. Chem. Phys.* **14** 5513-27

Hudson P K, Murphy D M, Cziczo D J, Thomson D S, de Gouw J A, Warneke C, Holloway J, Jost H-J and Hübler G 2004 Biomass-burning particle measurements: Characteristic composition and chemical processing **109**

IPCC 2014 *Contribution of Working Groups I, II and III to the Fifth Assessment Report of the Intergovernmental Panel on Climate Change [Core Writing Team, R.K. Pachauri and L.A. Meyer (eds.)]* (IPCC, Geneva, Switzerland

IPCC 2021 *Climate Change 2021: The Physical Science Basis. Contribution of Working Group I to the Sixth Assessment Report of the Intergovernmental Panel on Climate Change [Masson-Delmotte, V., P. Zhai, A. Pirani, S. L. Connors, C. Péan, S. Berger, N. Caud, Y. Chen, L. Goldfarb, M. I.*

Gomis, M. Huang, K. Leitzell, E. Lonnoy, J. B. R. Matthews, T. K. Maycock, T. Waterfield, O. Yelekçi, R. Yu and B. Zhou (eds.)] vol In Press.: Cambridge University Press.)

Jiang Y, Lu Z, Liu X, Qian Y, Zhang K, Wang Y and Yang X Q 2016 Impacts of global open-fire aerosols on direct radiative, cloud and surface-albedo effects simulated with CAM5 *Atmos. Chem. Phys.* **16** 14805-24

Jiang Y, Yang X-Q, Liu X, Qian Y, Zhang K, Wang M, Li F, Wang Y and Lu Z 2020 Impacts of Wildfire Aerosols on Global Energy Budget and Climate: The Role of Climate Feedbacks *Journal of Climate* **33** 3351-66

Kang S, Zhang Y, Qian Y and Wang H 2020 A review of black carbon in snow and ice and its impact on the cryosphere *Earth-Science Reviews* **210** 103346

Ke Z, Wang Y, Zou Y, Song Y and Liu Y 2021 Global Wildfire Plume-Rise Data Set and Parameterizations for Climate Model Applications **126** e2020JD033085

Koch D and Hansen J 2005 Distant origins of Arctic black carbon: A Goddard Institute for Space Studies ModelE experiment *Journal of Geophysical Research: Atmospheres* **110**

Koch D, Schmidt G A and Field C V 2006 Sulfur, sea salt, and radionuclide aerosols in GISS ModelE **111**

Liu J C, Pereira G, Uhl S A, Bravo M A and Bell M L 2015 A systematic review of the physical health impacts from non-occupational exposure to wildfire smoke *Environmental Research* **136** 120-32

Liu Y, Goodrick S and Heilman W 2014 Wildland fire emissions, carbon, and climate: Wildfire–climate interactions *Forest Ecology and Management* **317** 80-96

Macias Fauria M and Johnson E A 2006 Large-scale climatic patterns control large lightning fire occurrence in Canada and Alaska forest regions *Journal of Geophysical Research: Biogeosciences* **111**

Menon S, Del Genio A D, Kaufman Y, Bennartz R, Koch D, Loeb N and Orlikowski D 2008 Analyzing signatures of aerosol-cloud interactions from satellite retrievals and the GISS GCM to constrain the aerosol indirect effect **113**

Menon S, Koch D, Beig G, Sahu S, Fasullo J and Orlikowski D 2010 Black carbon aerosols and the third polar ice cap *Atmos. Chem. Phys.* **10** 4559-71

Metzger S, Mihalopoulos N and Lelieveld J 2006 Importance of mineral cations and organics in gas-aerosol partitioning of reactive nitrogen compounds: case study based on MINOS results *Atmos. Chem. Phys.* **6** 2549-67

Pechony O and Shindell D T 2009 Fire parameterization on a global scale *Journal of Geophysical Research* **114**

Price C and Rind D 1994 Modeling Global Lightning Distributions in a General Circulation Model *Monthly Weather Review* **122** 1930-9

Randerson J T, Chen Y, van der Werf G R, Rogers B M and Morton D C 2012 Global burned area and biomass burning emissions from small fires *Journal of Geophysical Research: Biogeosciences* **117**

Rayner N A, Parker D E, Horton E B, Folland C K, Alexander L V, Rowell D P, Kent E C and Kaplan A 2003 Global analyses of sea surface temperature, sea ice, and night marine air temperature since the late nineteenth century **108**

Schmidt G A, Kelley M, Nazarenko L, Ruedy R, Russell G L, Aleinov I, Bauer M, Bauer S E, Bhat M K, Bleck R, Canuto V, Chen Y-H, Cheng Y, Clune T L, Del Genio A, de Fainchtein R, Faluvegi

595 G, Hansen J E, Healy R J, Kiang N Y, Koch D, Lacis A A, LeGrande A N, Lerner J, Lo K K,
596 Matthews E E, Menon S, Miller R L, Oinas V, Oloso A O, Perlwitz J P, Puma M J, Putman W
597 M, Rind D, Romanou A, Sato M, Shindell D T, Sun S, Syed R A, Tausnev N, Tsigaridis K,
598 Unger N, Voulgarakis A, Yao M-S and Zhang J 2014 Configuration and assessment of the GISS
599 ModelE2 contributions to the CMIP5 archive *Journal of Advances in Modeling Earth Systems*
600 **6** 141-84
601 Shindell D T, Faluvegi G, Unger N, Aguilar E, Schmidt G A, Koch D M, Bauer S E and Miller R L 2006
602 Simulations of preindustrial, present-day, and 2100 conditions in the NASA GISS composition
603 and climate model G-PUCCINI *Atmos. Chem. Phys.* **6** 4427-59
604 Sofiev M, Ermakova T and Vankevich R 2012 Evaluation of the smoke-injection height from wild-land
605 fires using remote-sensing data *Atmos. Chem. Phys.* **12** 1995-2006
606 Tsigaridis K and Kanakidou M 2007 Secondary organic aerosol importance in the future atmosphere
607 *Atmospheric Environment* **41** 4682-92
608 Twomey S 1974 Pollution and the planetary albedo *Atmospheric Environment (1967)* **8** 1251-6
609 van der Werf G R, Randerson J T, Giglio L, van Leeuwen T T, Chen Y, Rogers B M, Mu M, van Marle
610 M J E, Morton D C, Collatz G J, Yokelson R J and Kasibhatla P S 2017 Global fire emissions
611 estimates during 1997–2016 *Earth Syst. Sci. Data* **9** 697-720
612 Veira A, Kloster S, Schutgens N A J and Kaiser J W 2015 Fire emission heights in the climate system –
613 Part 2: Impact on transport, black carbon concentrations and radiation *Atmos. Chem. Phys.* **15**
614 7173-93
615 Venevsky S, Thonicke K, Sitch S and Cramer W 2002 Simulating fire regimes in human-dominated
616 ecosystems: Iberian Peninsula case study *Global Change Biology* **8** 984-98
617 Wagner V 1987 *Development and structure of the Canadian Forest Fire Weather Index System, Forestry*
618 *Technical Report*: Canadian Forestry Service)
619 Walter C, Freitas S R, Kottmeier C, Kraut I, Rieger D, Vogel H and Vogel B 2016 The importance of
620 plume rise on the concentrations and atmospheric impacts of biomass burning aerosol *Atmos.*
621 *Chem. Phys.* **16** 9201-19
622 Ward D S, Kloster S, Mahowald N M, Rogers B M, Randerson J T and Hess P G 2012 The changing
623 radiative forcing of fires: global model estimates for past, present and future *Atmos. Chem. Phys.*
624 **12** 10857-86
625 Warren S G and Wiscombe W J 1980 A Model for the Spectral Albedo of Snow. II: Snow Containing
626 Atmospheric Aerosols %J Journal of Atmospheric Sciences **37** 2734-45
627 Xu L, Zhu Q, Riley W J, Chen Y, Wang H, Ma P-L and Randerson J T 2021 The Influence of Fire
628 Aerosols on Surface Climate and Gross Primary Production in the Energy Exascale Earth
629 System Model (E3SM) *Journal of Climate* **34** 7219-38
630 Yan H, Zhu Z, Wang B, Zhang K, Luo J, Qian Y and Jiang Y 2021 Tropical African wildfire aerosols
631 trigger teleconnections over mid-to-high latitudes of Northern Hemisphere in January
632 *Environmental Research Letters* **16** 034025
633 Yu P, Toon O B, Bardeen C G, Zhu Y, Rosenlof K H, Portmann R W, Thornberry T D, Gao R-S, Davis S
634 M, Wolf E T, Gouw J d, Peterson D A, Fromm M D and Robock A 2019 Black carbon lofts
635 wildfire smoke high into the stratosphere to form a persistent plume **365** 587-90
636 Yue X, Strada S, Unger N and Wang A 2017 Future inhibition of ecosystem productivity by increasing
637 wildfire pollution over boreal North America *Atmos. Chem. Phys.* **17** 13699-719
638 Yue X and Unger N 2015 The Yale Interactive terrestrial Biosphere model version 1.0: description,

639 evaluation and implementation into NASA GISS ModelE2 *Geosci. Model Dev.* **8** 2399-417
640 Yue X and Unger N 2018 Fire air pollution reduces global terrestrial productivity *Nature*
641 *Communications* **9** 5413
642 Zhuravleva T B, Kabanov D M, Nasrtdinov I M, Russkova T V, Sakerin S M, Smirnov A and Holben B
643 N 2017 Radiative characteristics of aerosol during extreme fire event over Siberia in summer
644 2012 *Atmos. Meas. Tech.* **10** 179-98
645 Zou Y, Wang Y, Qian Y, Tian H, Yang J and Alvarado E 2020 Using CESM-RESFire to understand
646 climate–fire–ecosystem interactions and the implications for decadal climate variability *Atmos.*
647 *Chem. Phys.* **20** 995-1020
648
649

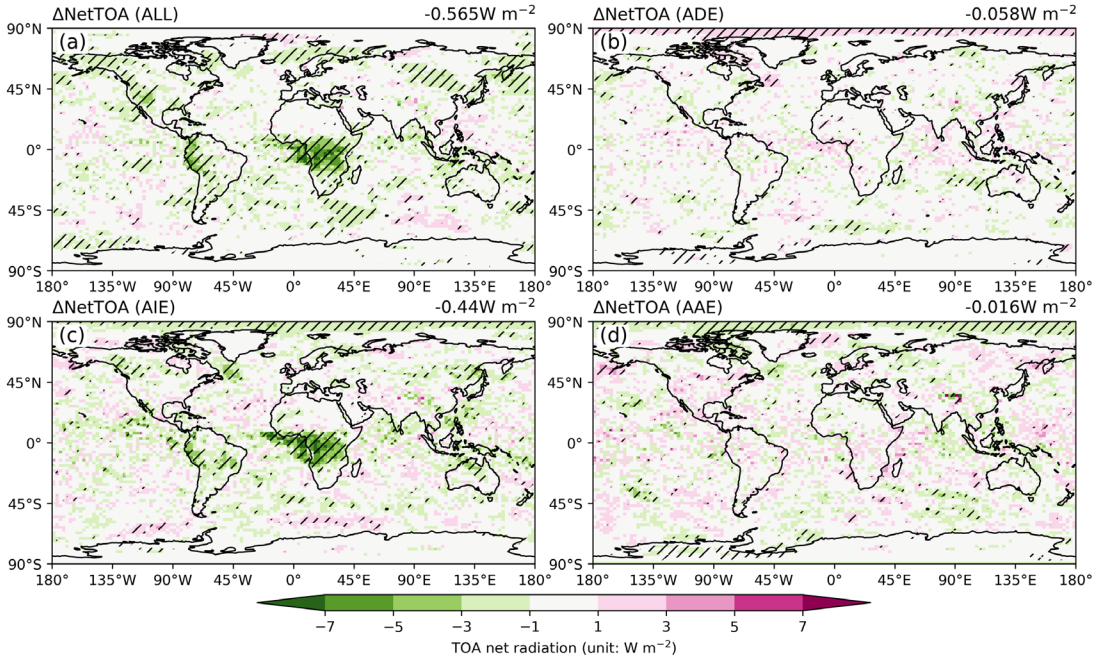

650

651 **Fig. 1** Changes in net radiation flux at top of atmosphere due to (a) total effects, (b) ADE, (c) AIE,
652 and (d) AAE of fire aerosols. Positive values represent the increase of downward radiation. Global
653 average value is shown at the top of each panel. Slashes denote areas with significant ($p < 0.1$)
654 changes.

655

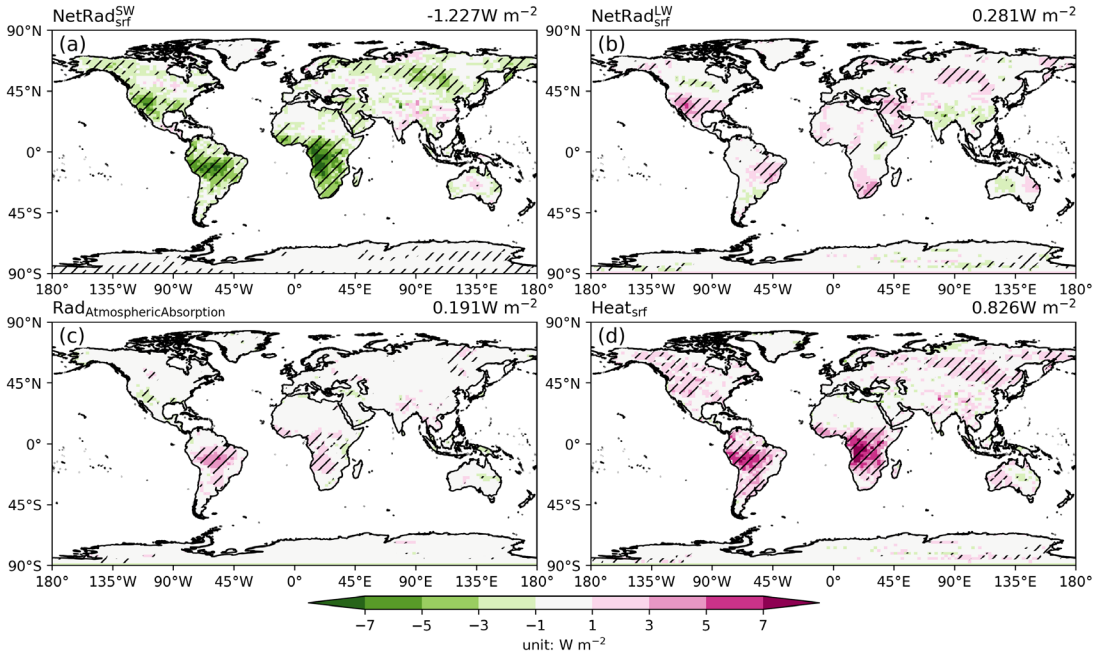

Fig. 2 Changes in (a) surface net shortwave radiation, (b) surface net longwave radiation, (c) atmospheric absorbed radiation, and (d) surface heat flux (sensible + latent) over land grids caused by fire aerosols. Positive values represent the increase of downward radiation/heat for (a, b and d) and absorption for (c). Global land average value is shown at the top of each panel. Slashes denote areas with significant ($p < 0.1$) changes.

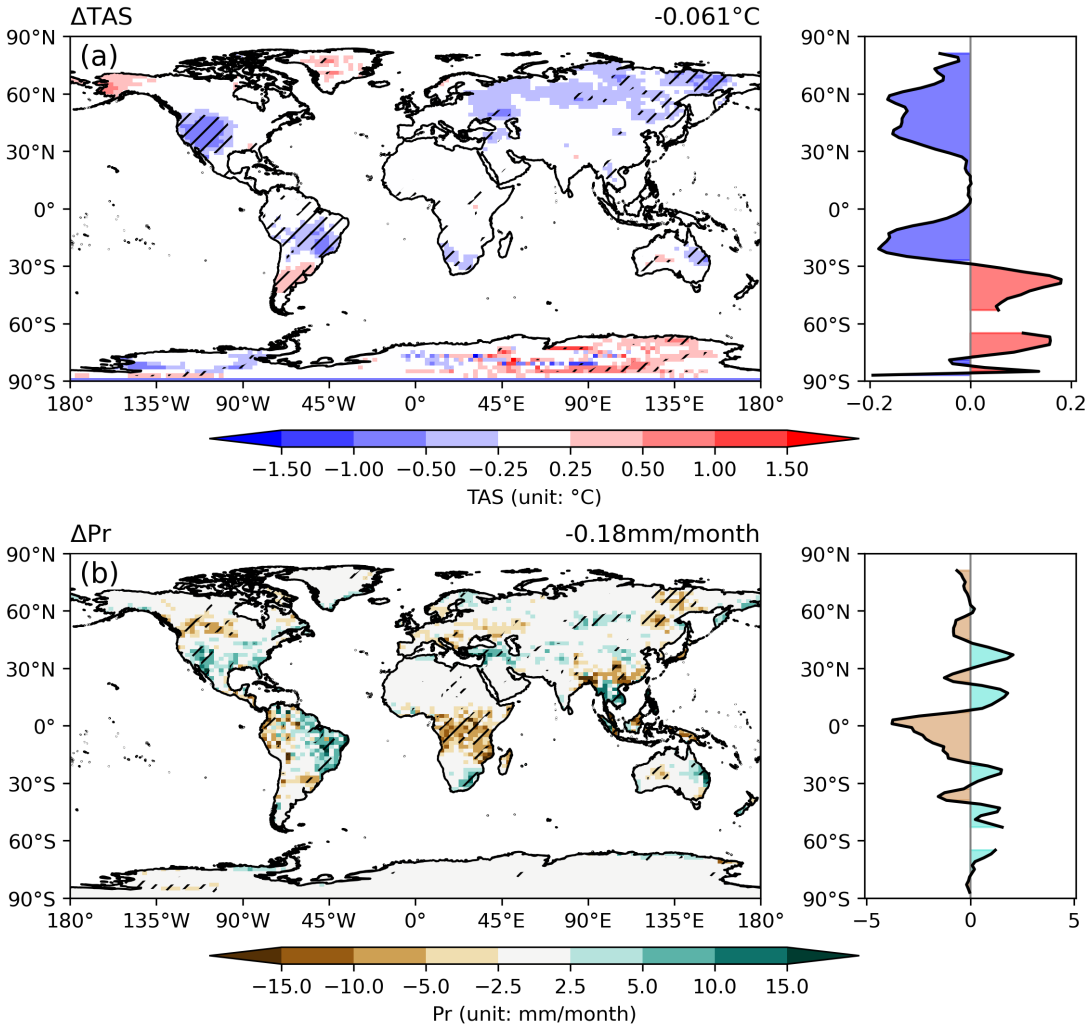

663

664 **Fig. 3** Changes in (a) surface air temperature and (b) precipitation over land grids caused by fire
665 aerosols. The zonal averages of these changes are shown by the side of each panel. Global land
666 average value is shown at the top of each panel. Slashes denote areas with significant ($p < 0.1$)
667 changes.

668

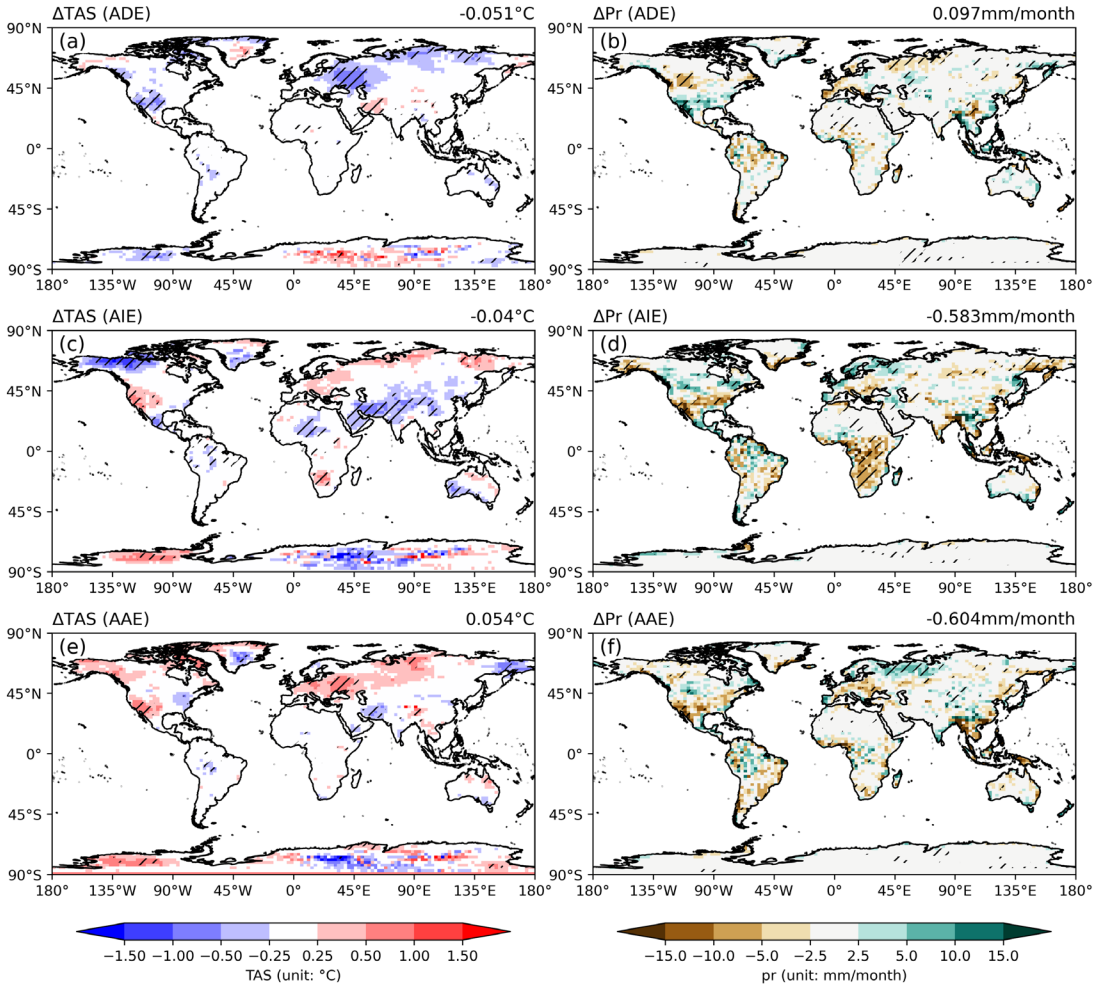

669
670 **Fig. 4** Changes in (a, c, e) surface air temperature and (b, d, f) precipitation over land grids due to
671 (a, b) ADE, (c, d) AIE, and (e, f) AAE of fire aerosols. Global land average value is shown at the
672 top of each panel. Slashes denote areas with significant ($p < 0.1$) changes.
673

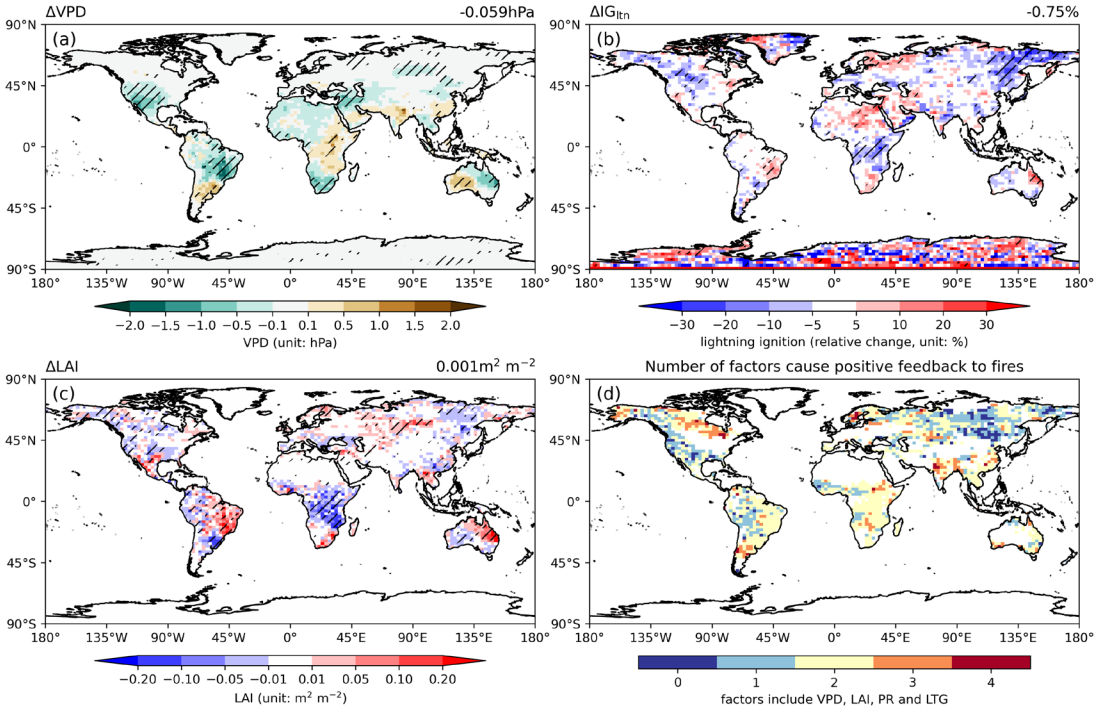

Fig. 5 Changes in (a) vapor pressure deficit (VPD), (b) lightning ignition, and (c) leaf area index (LAI) over land grids induced by fire aerosols. Global land average value is shown at the top of each panel. Slashes denote areas with significant ($p < 0.1$) changes. The number of factors whose changes induced by fire aerosols cause positive feedback to fire emissions is shown in (d). Only grids with fire-emitted OC larger than 1×10^{-12} kg s^{-1} m^{-2} (colored domain in Fig. S1b) are shown in (d).

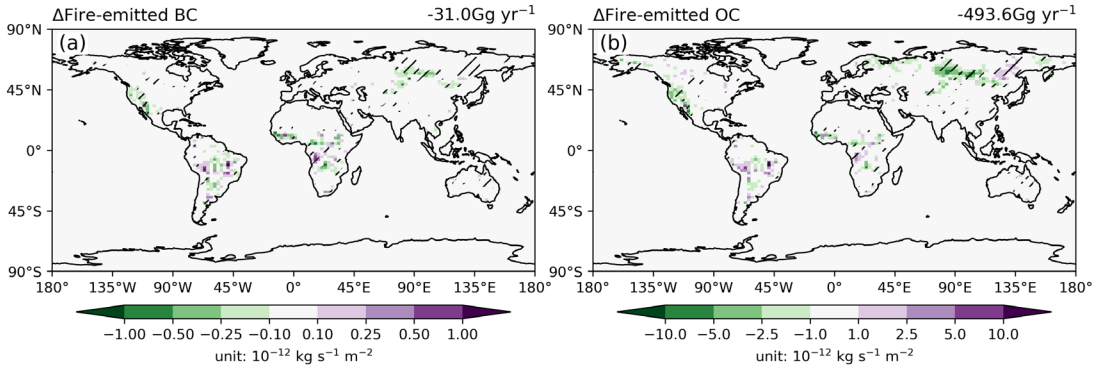

Fig. 6 Changes in fire emissions of (a) BC and (b) OC due to the fast response feedback. The changes of fire emissions are calculated as the differences between YF_AD_AI_AA and NF_AD_AI_AA with slashes indicating significant ($p < 0.1$) changes. The total emission is shown at the top of each panel.

687 **Table 1.** Summary of simulations using ModelE2-YIBs

Simulation	Fires [a]	Aerosol direct effect	Aerosol indirect effect	Aerosol albedo effect
NF_AD	No	Yes	No	No
YF_AD	Yes	Yes	No	No
NF_AD_AI	No	Yes	Yes	No
YF_AD_AI	Yes	Yes	Yes	No
NF_AD_AA	No	Yes	No	Yes
YF_AD_AA	Yes	Yes	No	Yes
NF_AD_AI_AA	No	Yes	Yes	Yes
YF_AD_AI_AA	Yes	Yes	Yes	Yes

688

689 [a] All simulations predict fire emissions but the runs with NF do not feed the fire aerosols into the
690 model to perturb radiative fluxes.

691

692 **Table 2.** Comparsion of the simulated fire-induced change in radiative forcings at TOA and
693 surface climate with previous studies

Reference	RF ($W\ m^{-2}$)	ADE ($W\ m^{-2}$)	AIE ($W\ m^{-2}$)	AAE ($W\ m^{-2}$)	TAS (°C)	Pr ($mm\ month^{-1}$)
Ward *et al.* (2012)[a]	-0.55	0.10	-1.00	0.00	—	—
Heald *et al.* (2014)	—	-0.19	—	—	—	—
Veira *et al.* (2015)	—	-0.20	—	—	—	—
Grandey *et al.* (2016)	-1.0	0.04	-1.11	-0.1	—	-0.018
Jiang *et al.* (2016)	-0.51	0.16	-0.70	0.03	-0.03	-0.3
Zou *et al.* (2020)	-0.59	-0.003	-0.82	0.19	—	—
Xu *et al.* (2021)	-0.73	0.25	-0.98	—	-0.17	-1.2
Yan *et al.* (2021)	-0.62	0.17	-0.74	-0.04	0.03	—
This study	-0.565	-0.058	-0.440	-0.016	-0.061	-0.180

694
695 [a] other effects of fire-induced on radiative turbulances are considered in this paper